E-band millimeter wave indoor channel characterization

Aliou Bamba, Francesco Mani, Raffaele d'Errico

E-Band Millimeter Wave Indoor Channel Characterization

Aliou Bamba*,†, Francesco Mani*,† and Raffaele D'Errico*,†
*CEA, LETI, Minatec Campus, 17 rue des Martyrs, 38054 Grenoble, France
†Université Grenoble-Alpes, Grenoble, France

***Abstract*—This paper presents the channel characterization of indoor environments in the E-Band (80.5-86.5 GHz). Measurements were performed by means of mechanical steering of directive antennas at both the transmitter and receiver side, allowing a double-directional angular characterization. Specular components have been estimated by means of a detection algorithm. Characterization of the path loss, delay spread, Angle-of-Departure and Angle-of-Arrival spreads are presented for two indoor environments.**

I. Introduction

The number of wirelessly connected devices along with the number of users are exponentially increasing nowadays owning to, e.g., the advent of tablets and smartphones. The 5th Generation of mobile communications (5G) is expected to offer extreme broadband, pervasive and large connectivity with very low latency [1]. The usual frequency bands for mobile communications systems (i.e., 300 MHz-6 GHz) can not provide satisfactory quality of service due to the limited bandwidth therein. Therefore, the World Radio-communications Conference (WRC) 2015 identified several of the millimeter wave (mmW) bands for further study for mobile applications [2]. The use of these frequency bands will considerably increase the channel capacity due to the large available bandwidth. However, the radio channel ought to be well understood at the millimeter frequencies by the designers of future communications systems. Indeed, the knowledge of the channel state information is important in order to design efficient and optimal communications systems. The path loss models are important for predicting the received signal strength at any location in the considered environment whereas the path loss exponent gives an extent of the coverage. The delay dispersion - rms delay spread - is needed to assess the maximum achievable throughput without equalization. The space selectivity information (i.e., angular spread) of an environment is a prerequisite to achieve optimal beamforming for directive antennas elements in MIMO systems [3]. Moreover, the angular spread provides crucial information such as the fading rate of the signal, the cross-correlation function in MIMO systems [4].

The development of integrated circuits components and small-size antennas at mmW [5] has triggered researchers' interest to investigate the propagation mechanisms at mmW frequencies. Several researches [6]–[14] have thus addressed the radio channel characteristics in the mmW frequencies. The mmW multipaths clustering for double directional channel [11], the spatial and temporal characteristics [7] and the shadowing by human bodies [10] have been investigated around 60 GHz in indoor environments. Most of the studies in channels characterization and modelling at mmW frequencies have been conducted in the 60 GHz band, being a worldwide license free band. Nevertheless, the characterization and modeling of the radio channel parameters is not limited to these frequencies [6], [15], [16]. To the best of the authors' knowledge, not many studies have dealt with channel measurements in the 82 GHz frequency. Only [17] has presented channel characterization results in roof-to-street and street canyon scenarios. We present here the channel measurement results in indoor environments in the 82 GHz band identified in [2] along with the preliminary results of the channel characterization. The paper is organized as follows: the measurement system and scenarios are presented in Section II. The methodology is introduced in Section III. Next, the measurement results and discussions are presented in Section IV. Finally, Section V concludes the paper.

II. Environment and measurement description

A. Environment description

The measurement campaign has been carried out at CEA-Leti in two scenarios: office and conference room. Photos of the scenarios are shown in Figure 1.

The first scenario is a classical office of approximately 50 m^2 with desks, storage cabinets and bookshelves (furniture was arranged at the sides of the room leaving a large empty part in the center where there was enough space to perform the measurements). The room dimensions are approximately $7\ m \times 7\ m \times 2.6\ m$. A floor plan of the office is depicted in Fig. 2a, along with the locations of the terminals. The second scenario is a conference room of approximately 85 m^2. Its furniture is composed by five rows of chairs and few storage closets. There is a stage, equipped with tables, chairs and a podium for the speaker, 20 cm elevated with respect to the ground. A floor plan of the room is shown in Fig. 2b, together with the locations of the measurement points.

B. Measurement setup

A 4-port Vector Network Analyzer (VNA) has been used to record the measurements. To be able to measure at 82 GHz, frequency converters have been employed at both sides. These converters work as frequency multipliers, as they are able to convert frequencies from the range between 10 and 15 GHz

Fig. 1: Pictures of the two measurement scenarios: office (left) and conference (right) room

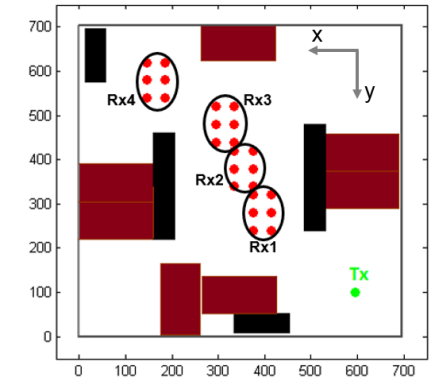

(a)

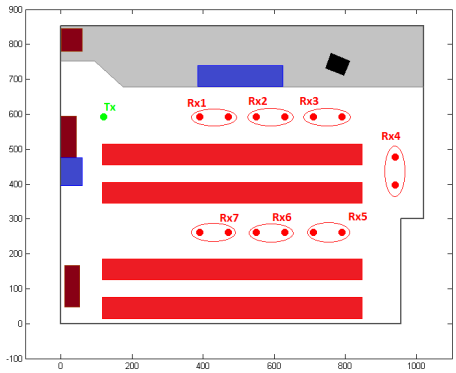

(b)

Fig. 2: Floor plan of the scenarios with measurement grids: (a) office and (b) conference room. Each location is comprised of 6 (resp. 2) positions in the office (resp. conference room)

to the range between 60 and 90 GHz. The measurements were carried out in a 6 GHz band between 80.5 and 86.5 GHz. The power emitted by the converters is typically 3 dBm for an input power of 7 dBm. The setup parameters for this measurement campaign are presented in Table I. With these parameters, the maximum recorded delay is 333.33 ns which corresponds to a distance of 100 m. The low IF bandwidth permits us to have a noise floor of approximately -140 dB.

Parameter	Value
Start frequency	80.5 GHz
Stop frequency	86.5 GHz
No. sweep points	2001
IF bandwidth	100 Hz
Averaging	1
Azimuth step (Tx, Rx)	(45°, 10°)

TABLE I: VNA setup and antennas directional parameters

Directional antennas have been used for the measurements. At the transmitter (Tx) side, we used a vertically polarized standard horn antenna with 10 dBi gain and approximately 50° half power bandwidth (HPBW) in the frequency band under investigation. At the receiver (Rx) side, instead, a vertically polarized standard horn with 20 dBi gain and HPBW of 16° was used. To fully investigate the channel in the azimuth domain, two positioner devices have been used to rotate the antennas and perform mechanical steering. Given the different HPBW it was chosen to perform mechanical steering by step 45° for the Tx, and 10° for the Rx. At each measured position, a full 360° steering was performed on both Tx and Rx sides. Additionally, the rotating motor at Rx side is collocated with a 2D positioner that is able to scan in a grid of 80×80 cm^2. At each Rx location in the office, the 2D positioner moved following a 2×3 grid with 40 cm step and the channel is probed at each position (see Fig. 2a). In the conference room, only one of the two axes is used and each grid is composed by two points separated by 80 cm (see Fig. 2b).

III. Multipath Detection Algorithm

For each scanning direction of the Tx and Rx, (Ω_s^T, Ω_s^R), the recorded channel frequency response is $H_p(f, \Omega_s^T, \Omega_s^R)$. The raw channel impulse response is obtained by inverse Fourier transform of the frequency response multiplied by an energy normalized Hamming window function $W(f)$ to reduce side-lobe effects. For each acquisition the antenna gain at Tx and Rx side was removed in order to obtain the channel impulse response $h_p(\tau, \Omega_s^T, \Omega_s^R)$ and the power angular delay profile (PADP):

$$PADP(\tau, \Omega_s^T, \Omega_s^R) = |h_p(\tau, \Omega_s^T, \Omega_s^R)|^2 \quad (1)$$

Following the approach described in [13], [18], extended to the double-directional channel, the synthetic omnidirectional power delay profile (PDP) is then obtained as follows:

$$PDP_p(\tau) = \frac{1}{N_s^T N_s^R} \sum_{T=1}^{N_s^T} \sum_{R=1}^{N_s^R} PADP(\tau, \Omega_s^T, \Omega_s^R) \quad (2)$$

where N_s^T (resp. N_s^R) is the number of scanning direction of the Tx (resp. Rx).

The number of detectable paths (N_k) and their corresponding delays τ_k, ($k = \{1...N_k\}$) is determined from the synthetic $PDP_p(\tau)$ by applying the path detection algorithm defined in [13]. The algorithm searches for local maxima in the syn-

thetic omnidirectional PDP by comparison with the threshold function defined as:

$$T(\tau) = \frac{\varepsilon}{\Delta} \int_{\tau - \frac{\Delta}{2}}^{\tau + \frac{\Delta}{2}} PDP_p(x)dx \tag{3}$$

where Δ is the sliding window length and ε is a threshold offset.
A peak is identified as specular path at $\tau = \tau_k$ if $PDP_p(\tau_k) > T(\tau_k)$. It is important to accurately find the right values for these two parameters in a way that it allows us to find all the relevant paths and, at the same time, to avoid to detect artifacts. In our case, we used ε=3 dB and Δ=1.66 ns (i.e., 10 times the delay resolution). Each delay τ_k corresponds to a detected path and is mapped to a unique (Ω_s^T, Ω_s^R) couple defining the direction of departure and arrival of the k^{th} detected path. Knowing these estimates, the propagation channel impulse response can be reconstructed as follows:

$$\tilde{h}_p(\tau, \Phi^T, \Phi^R) = \sum_{k=1}^{N_k} \alpha_k \delta(\tau - \tau_k)\delta(\Phi^T - \Phi_k^T)\delta(\Phi^R - \Phi_k^R) \tag{4}$$

When a path is found at τ_k, the corresponding power is given by the following maximization function:

$$\alpha_k^2 = \max_{(\Phi_s^T, \Phi_s^R)} PADP(\tau_k, \Phi_s^T, \Phi_s^R) \tag{5}$$

where $R = 1...N_s^R$ and $T = 1...N_s^T$. Furthermore, the angle of arrival (AoA) and departure (AoD) of the k^{th} path is given by the couple (Φ_s^T,Φ_s^R) maximizing (5).
Fig. 3 shows an example of a synthetic PDP along with the detected multipaths. The polar plots - in terms of angles of arrival - of the two measurement scenarios are shown in Fig. 4.

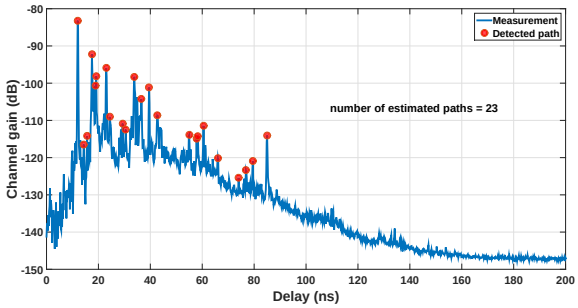

Fig. 3: Measured power delay profile in the office and the detected specular paths. The noise threshold is set to -130 dB.

IV. Measurement results and discussions

In this section, we provide the channel parameters derived from the measurement campaign in terms of path loss, angular and delay spread. All of them are computed only starting from the specular paths detected by the algorithm described in the previous section.

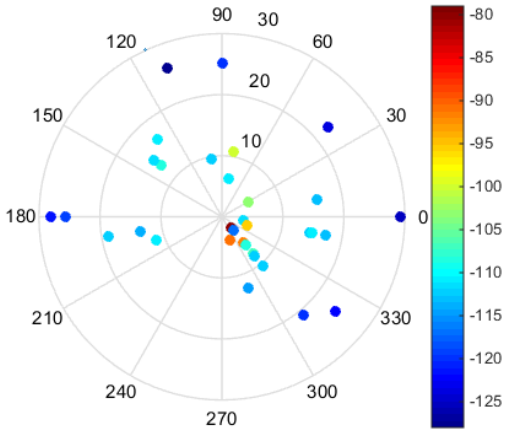

(a) Angle of arrival at Rx1 location (position 6). N_k=34 and σ_Φ=0.28

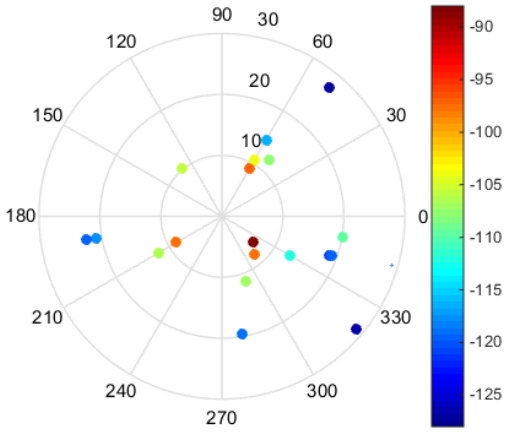

(b) Angle of arrival at Rx4 location (position 4). N_k=19 and σ_Φ=0.71

Fig. 4: Polar plot of the angles of arrival for two Rx locations in the office. The concentric circles indicate the path length in meters whereas the colors indicate the received paths strength

A. *Path loss model*

Path loss models are important features that provide information allowing efficient design of communications systems. For instance, the path loss model can be used to foresee the received power at any distance in a given environment. The relative received power P_t is obtained from the power integration of the detected paths:

$$P_t = \sum_{k=1}^{N_k} \alpha_k^2, \tag{6}$$

To model the path loss, we classically use the following equation:

$$PL(d)[dB] = PL_0 + 10\widehat{n}\log_{10}\left(\frac{d}{d_0}\right) + X_\sigma \tag{7}$$

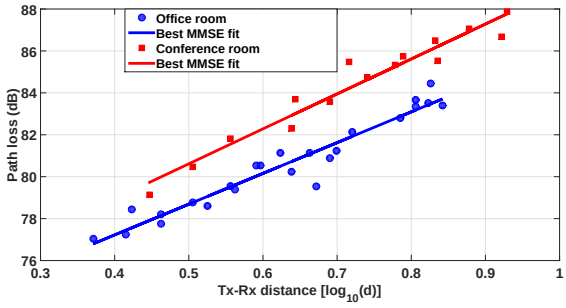

Fig. 5: Path loss model in the investigated office and conference rooms. In each case, the solid line is obtained with the MMSE estimator.

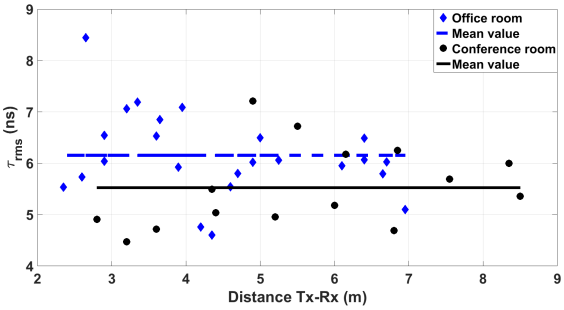

Fig. 6: Measured values of the rms delay spread as a function of Tx-Rx separation.

	PL_0 (dB)	$\widehat{n}$	X_σ
Office room	71.35	1.47	$\mathcal{N}(0,\ 0.55$ dB)
Conference room	72.30	1.67	$\mathcal{N}(0,\ 0.58$ dB)

TABLE II: Path loss model parameters

where PL_0 is the intercept in dB and $\widehat{n}$ is the path loss exponent that characterizes the increase in the channel path loss as a function of the Tx-Rx distance d. d_0 is the reference distance and set to 1 m. Both PL_0 and $\widehat{n}$ are obtained from the intercept and slope of the best-fit to (7) according to the minimum mean square error (MMSE) criteria. Finally, X_σ represents the shadowing loss.

Fig. 5 displays the measured path loss along with the path loss model expressed by (7) for both indoor environments shown in Fig. 2.

From the MMSE estimator and (7), an intercept PL_0 of about 71.35 dB (resp. 72.30 dB) and a path loss exponent ($\widehat{n}$) of 1.47 (resp. 1.67) are obtained for the office (resp. conference) room environment. It follows that X_σ is a normally distributed random variable with a mean of 0 dB in both environments and a standard deviation of 0.55 dB (resp. 0.58 dB) in the office (resp. conference) room, (i.e., $X_\sigma \sim \mathcal{N}(0,\ 0.55$ dB) in the office room and $X_\sigma \sim \mathcal{N}(0,\ 0.58$ dB) in the conference room). The parameters of the path loss model are summarized in Table II for both environments. A larger value of $\widehat{n}$ indicates that the path loss increases rapidly as the Tx-Rx distance increases. Path loss exponent values smaller than 2 - free space path loss - are obtained in the two investigated environments. This is due to the multiple paths reflected from the sidewalls, ceiling, floor (waveguide effect) and from the surrounding scatterers. The reflected and scattered paths contribute to the total received power, and hence reduce the path loss exponent in both environments. Moreover, in comparison to the office scenario, the higher path loss exponent in the conference room is due to the longer traveled distance of the paths (reflected, scattered, and so on), which in turn increase the path loss.

Similar values of the path loss exponent as in Table II ($\widehat{n} < 2$) have been obtained in indoor environments in the literature. A path loss exponent of 1.2 and 1.8 are obtained in a corridor and office environment, respectively, at 28 GHz [15]. Measurements in an office lead to a path loss exponent of 1.92 at 60 GHz [19]. [20] obtained a path loss exponent of 1.3 at 73 GHz. Similarly to our scenarios, note that these values have been determined for measurements in LOS conditions. Measurements in NLOS scenarios show larger values of the path loss exponent [15], [19], [20].

B. Delay spread

One of the important delay parameters is the root mean square (rms) delay spread (τ_{rms}). This parameter gives an extent of the delay dispersion of the multipaths arriving at the Rx and provides also an estimation of the coherence bandwidth of the channel. The shorter the delay spread is, the lesser will be the need of equalization. It is obtained as follows:

$$\tau_{rms} = \sqrt{\frac{\sum_{k=1}^{K}(\tau_k - \tau_m)^2\alpha_k^2}{\sum_{k=1}^{K}\alpha_k^2}} \tag{8}$$

where τ_m is the mean arrival delay of the multipaths and is defined as follows:

$$\tau_m = \frac{\sum_{k=1}^{K}\alpha_k^2\tau_k}{\sum_{k=1}^{K}\alpha_k^2} \tag{9}$$

K, α_k^2, and τ_k are the number of detected specular paths, the power of the k^{th} path and the delay of arrival of the k^{th} path, respectively.

The rms delay spread values throughout the office and conference room are depicted in Fig. 6. The τ_{rms} varies from 4.60 ns to 8.40 ns for the office and from 4.47 ns to 7.20 ns for the conference room and there is clearly no trend between these values and the Tx-Rx distance. Therefore, an environment is characterized by the mean rms delay spread, which is approximately 6.1 ns and 5.5 ns for the office and conference room, respectively. Moreover, we can visually see that the τ_{rms} values are randomly scattered around the mean value. Therefore, the actual rms delay spread of the environment can be thought of as the summation of a constant rms delay spread (i.e., the mean value), plus a random variable (X_τ) expressing the variations around the mean value. From the measurements, we found that $X_\tau \sim \mathcal{N}(0,\ 0.83$ ns) for the office and $X_\tau \sim \mathcal{N}(0,\ 0.80$ ns) for the conference room.

We notice that the mean rms delay spread is slightly larger

in the office than that in the conference room. This might be caused by the waveguide effect - more important in the office - and the presence of many scatterers that favor the rise of multipaths. Hence, the power level in the office room is higher than that in the conference room where it drops faster in the noise, justifying the lower value of the rms delay spread.
The rms delay spread values that we obtain agree with results reported in the literature. Rms delay spread values ranging from 3 to 15 ns, and 2 to 12 ns are obtained [21] at 70 GHz in an office room and shopping mall, respectively. An average rms delay spread of 3.30 is measured in a typical office at 73 GHz [20]. Measurements of rms delay spread reported values between 5 and 15 ns with a mean value of 8.80 ns at 58 GHz in an indoor environment [22].

C. Angular spread

Similarly to the delay spread, the angular spread is also an important parameter in MIMO systems. It shows the extent of the space selectivity, and hence is related to the space correlation in multiple antennas systems. Further practical uses of the angular spread in communications systems can be found in [3], [4], [24]. Note that we only consider the azimuth plane, and let Φ_k be the arrival (or departure) azimuth angle of the k^{th} multipath. The angular spread is defined as follows [24].

$$\sigma_\Phi = \sqrt{\frac{\sum_{k=1}^{K} |e^{j\Phi_k} - \mu_\Phi|^2 \alpha_k^2}{\sum_{k=1}^{K} \alpha_k^2}} \tag{10}$$

where μ_Φ is the mean arrival (or departure) azimuth, and is defined as:

$$\mu_\Phi = \frac{\sum_{k=1}^{K} \alpha_k^2 e^{j\Phi_k}}{\sum_{k=1}^{K} \alpha_k^2} \tag{11}$$

Note that μ_Φ is a complex number and $\mid \mu_\Phi \mid \leq 1$. The departure and arrival angular spread values for the two investigated environments are shown in Fig. 7. The angular spread calculated in this way varies between 0 and 1, with 0 indicating that the multipaths arrive (or depart) in a single direction whereas 1 indicates that there is no preference in the directions of departure (or arrival) of the multipaths [4], [24], [25].
From our measurements, the departure (resp. arrival) angular spread values are within the range [0.46, 0.75] (resp. [0.28, 0.79]), depending on the terminals' location in the office room (Fig. 7a). For the conference room, the departure (resp. arrival) angular spread values range from 0.33 to 0.96 (resp. from 0.2 to 0.56) as shown in Fig. 7b. We clearly also see that the departure angular spread values are larger than the arrival ones for both environments. This is because the Tx kept the same location - close to sidewalls - whereas the Rx occupied several locations throughout the environments. In the office room, the highest values of the arrival angular spread are obtained for the Rx4 location. This location was close to the upper left corner of the office (see Fig. 2a). Moreover, Rx4 is surrounded by multiple pieces of furniture, e.g. a metallic closet, two desks with computers, et cetera. The relatively small values of the arrival angular spread for the three other locations are

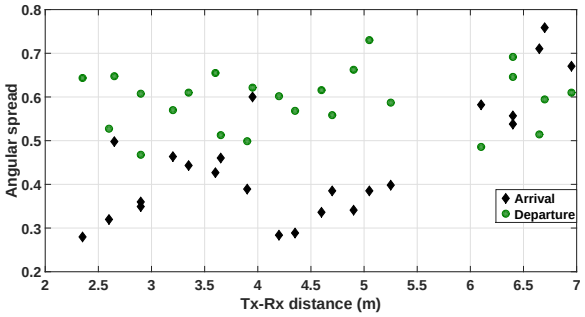

(a) Office room

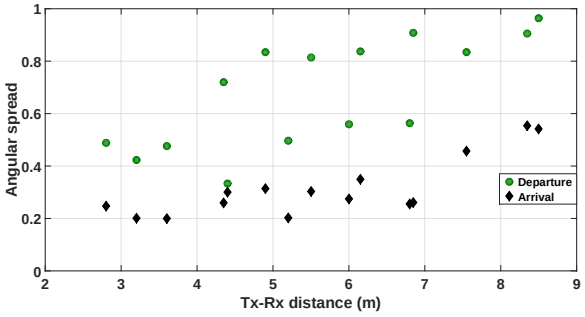

(b) Conference room

Fig. 7: Estimated angular spread at Tx and Rx side

explained by their positions in the center of the room, thus far from the walls and other scatterers and most of the multipaths come in favored directions (see Fig. 4a). On the contrary, it is difficult to define a preferred arrival angle of the multipath when the angular spread becomes higher (see Fig. 4b).
Lower values of the arrival angular spread have been found in the conference room with values ranging from 0.20 to 0.56 as shown in Fig. 7b. This can be explained by two reasons: *i)* there are less scatterers in the conference room and *ii)* the conference room is more spacious than the office room. The waves arrive in favorite directions when the room volume increases, i.e., the density of the scatterers decreases. The extreme case of this observation will occur in an outdoor environment where very low values of the angular spread are expected. Reported angular spread values at 60 GHz in various environments (from outdoor to indoor) [7] support our observation. However, note that the higher value of the angular spread in the conference room occurs when the receiver is the closest to a wall (i.e., Rx_4), as already noticed in the office room.

V. Conclusion

A measurement campaign with directive antennas has been carried out in two indoor environments at 82 GHz. This made possible to use a detection algorithm to derive multipath components. A path loss model is evaluated, providing path loss exponents of 1.47 and 1.67 for the office and conference room, respectively. The channel dispersion in the delay and angular domain has been investigated. A mean rms delay

spread value of 6.1 ns is obtained and departure (resp. arrival) angular spread values ranging from 0.46 to 0.75 (resp. 0.28 to 0.79) are obtained for the office room. For the conference room, a mean rms delay of 5.50 ns and angular spread values from 0.20 to 0.56 are obtained. The highest arrival angular spread occurs for Rx location close to scatterers and corners whereas locations in the middle of the room show lower dispersion of the AoA. Our experimental results are compared with values from the literature and satisfactory agreements are obtained.

ACKNOWLEDGMENT

The research leading to these results received funding from the European Commission H2020 programme under grant agreement 671650 (mmMagic Project).

REFERENCES

[1] C. Dehos and J. L. González and A. D. Domenico and D. Kténas and L. Dussopt. Millimeter-wave access and backhauling: the solution to the exponential data traffic increase in 5G mobile communications systems? *IEEE Communications Magazine*, 52(9):88–95, September 2014.

[2] The ITU weblink to WRC 15. http://www.itu.int/en/ITU-R/ conferences/wrc/2015/Pages/default.aspx,, 2015. [Online].

[3] M. Sanchez-Fernandez, S. Zazo, R. Valenzuela. "Performance comparison between beamforming and spatial multiplexing for the downlink in wireless cellular systems". *IEEE Trans. Wireless Commun.*, 6(7): pages 2427–2431, July 2007.

[4] G. D. Durgin, and T. S. Rappaport. "Effects of Multipath Angular Spread on the Spatial Cross-Correlation of Received Voltage Envelopes". In *IEEE 49th Vehicular Technology Conference*, volume 2, pages pages 996–1000, May 1999.

[5] T.S. Rappaport, J. N. Murdock, and F. Gutierrez. "State of the art in 60-GHz integrated circuits and systems for wireless communications". *Proceedings of the IEEE*, 99(8): pages 1390–1436, August 2011.

[6] D. Beauvarlet, and K. L. Virga. "Measured Characteristics of 30 GHz Indoor Propagation Channels With Low-Profile Directional Antennas". *IEEE Antennas Wireless Propag. Lett.*, 1: pages 87–90, 2002.

[7] H. Xu, V.Kukshya, T. S. Rappaport. "Spatial and Temporal Characteristics of 60-GHz Indoor Channels". *IEEE Journal on Selected Areas in Communications*, 20(3): pages 620–630, April 2002.

[8] S. Geng, J. Kivinen, X. Zhao, and P. Vainikainen. "Millimeter-Wave Propagation Channel Characterization for Short-Range Wireless Communications". *IEEE Trans. Veh. Technol.*, 58(1): pages 3–13, January 2009.

[9] M. Kyrö, K. Haneda, J. Simola, K. Takizawa, H. Hagiwara, and P. Vainikainen. "Statistical Channel Models for 60 GHz Radio Propagation in Hospital Environments". *IEEE Trans. Antennas Propag.*, 60(3): pages 1569–1577, March 2012.

[10] C. Gustafson, and F. Tufvesson. "Characterization of 60 GHz Shadowing by Human Bodies and Simple Phantoms". In *IEEE 6th European Conference on Antennas and Propagation (EUCAP)*, pages pages 473–477, 2012.

[11] C. Gustafson, K. Haneda, S. Wyne, and F. Tufvesson. "On mm-Wave Multipath Clustering and Channel Modeling". *IEEE Trans. Antennas Propag.*, 62(3): pages 1445–1455, February 2014.

[12] S. Häfner, D. A. Dupleich, R. Müller, J. Luo, E. Schulz, C. Schneider, R. S. Thomä, X. Lu, and T. Wang. "Characterization of Channel MEasurements at 70 GHz in Indoor Femtocells". In *IEEE 81s Vehicular Technology Conference*, pages pages 1–5, May 2015.

[13] K. Haneda, J. Järveläinen, A. Karttunen, M. Kyrö, and J. Putkonen. "A Statistical Spatio-Temporal Radio Channel Model for Large Indoor Environments at 60 and 70 GHz". *IEEE Trans. Antennas Propag.*, 63(6): pages 2694–2704, June 2015.

[14] W. Fan, I. Carton, J. Ø. Nielsen, K. Olesen, and G. Pedersen. "Measured wideband characteristics of indoor channels at centimetric and millimetric bands". *EURASIP Journal on Wireless Communications and Networking*, 2016:58, 2016.

[15] M. Lei, J. Zhang, T. Lei, D. Du. "28-GHz Indoor Channel Measurements and analysis of Propagation Characteristics". In *25th IEEE Int. Symp. on Pers., Indoor and Mobile Radio Commun.*, pages pages 208–212, 2014.

[16] J. Zhu, H. Wang, and W. Hong. "Large-Scale Fading Characteristics of Indoor channel at 45 GHz Band". *IEEE Antennas Wireless Propag. Lett.*, 14: pages 735–738, 2015.

[17] M. Kyrö, S. Ranvier, V. M. Kolmonen, K. Haneda, and P. Vainikainen. "Long Range Wideband Channel Measurements at 81-86 GHz Frequency Range". In *4th European Conference on Antennas and Propagation (EUCAP)*, pages pages 1–5, Barcelona, April 2010.

[18] T. S. Rappaport, G. R. MacCartney, M. K. Samimi, and S. Sun. "Wideband Millimeter-Wave Propagation Measurements and Channel Models for Future Wireless Communication System Design". *IEEE Trans. Commun.*, 63(9): pages 3029–3056, May 2015.

[19] N. Fryziel, C. Loyez, L. Clavier, N. Rolland, and P. A. Rolland. "Pathloss Model of the 60 GHz Indoor Radio Channel". *Microw. Opt. Technol. Lett.*, 34(3): pages 158–162, June 2002.

[20] S. Deng, M. K. Samimi, T. S. Rappaport. "28 GHz and 73 GHz MiMillimeter-Wave Indoor Propagation Measurements and Path Loss Models". In *IEEE International Conference on Communications (ICC), ICC Workshops*, 2015.

[21] K. Haneda, J. Järveläinen, A. Karttunen, M. Kyrö, and J. Putkonen. "Indoor Short-Range Radio Propagation Measurements At 60 and 70 GHz". In *8th European Conference on antennas and Propagation (EuCAP)*, 2014.

[22] H.Yang, P. F. M. Smulders, and M. H. A. J. Herben. "Indoor Channel Measurements and Analysis in the Frequency Bands 2 GHz and 60 GHz". In *IEEE 16th International Symposium on Personal, Indoor and Mobile Radio Communications (PIMRC)*, 2005.

[23] C. R. Anderson, and T. S. Rappaport. "In-Building Wideband Partition Loss Measurements at 2.5 and 60 GHz". *IEEE Trans. Wireless Commun.*, 3(3): pages 922–928, May 2004.

[24] B. H. Fleury. "First- and Second-Order Characterization of direction Dispersion and space Selectivity in the Radio Channel". *IEEE Trans. Inf. Theory*, 46(6): pages 2027–2044, September 2000.

[25] G. D. Durgin, and T. S. Rappaport. "Theory of Multipath shape Factors for Small-Scale Fading Wireless Channels". *IEEE Trans. Antennas Propag.*, 48(5): pages 682–693, May 2000.